Planar surface implanted diffractive grating couplers in SOI

R. Topley,[1,*] L. O'Faolain,[2] D. J. Thomson,[1] F. Y. Gardes,[1] G. Z. Mashanovich,[1] and G. T. Reed[1]

[1]*Optoelectronics Research Centre, University of Southampton, UK*
[2]*SUPA, School of Physics and Astronomy, University of St. Andrews, UK*
[*]*R.Topley@Soton.ac.uk*

Abstract: Grating couplers are used to efficiently couple light from an optical fibre to a silicon waveguide as they allow light to be coupled into or out from any location on the device without the need for cleaving. However, using the typical surface relief grating fabrication method reduces surface planarity and hence makes further processing more difficult. The ability to manufacture high quality material layers on top of a grating coupler allows multiple active optical layers to be realized for multi-layer integrated optical circuits, and may enable monolithic integration of optical and electronic circuits on separate layers. Furthermore, the nature of the refractive index change may enable removal via rapid thermal annealing for wafer scale testing applications. We demonstrate for the first time a coupling device utilising a refractive index change introduced by lattice disorder. Simulations show 44% of the power can be extracted from the waveguide by using uniform implanted gratings, which is not dissimilar to the performance of typical uniform surface relief gratings currently used. Losses determined empirically, of 5.5dB per coupler have been demonstrated.

OCIS codes: (050.1950) Diffraction gratings; (130.0130) Integrated optics; (230.0230) Optical devices; (050.0050) Diffraction and gratings.

References and links

1. G. T. Reed and A. P. Knights, *Silicon Photonics: An Introduction* (John Wiley, 2004).
2. F. Van Laere, T. Claes, J. Schrauwen, S. Scheerlinck, W. Bogaerts, D. Taillaert, L. O'Faolain, D. Van Thourhout, and R. Baets, "Compact focusing grating couplers for silicon-on-insulator integrated circuits," IEEE Photonics Technol. Lett. **19**(23), 1919–1921 (2007).
3. C. Kopp and A. Chelnokov, "Fiber grating couplers for silicon nanophotonic circuits: Design modeling methodology and fabrication tolerances," Opt. Commun. **282**(21), 4242–4248 (2009).
4. J. M. Steigerwald, S. P. Murarka, and R. J. Gutmann, *Chemical Mechanical Planarization of Microelectronic Materials* (Wiley, 2008).
5. T. M. B. Masaud, A. Tarazona, E. Jaberansary, X. Chen, G. T. Reed, G. Z. Mashanovich, and H. M. H. Chong, "Hot-wire polysilicon waveguides with low deposition temperature," Opt. Lett. **38**(20), 4030–4032 (2013).
6. D. J. Eaglesham and M. Cerullo, "Low-temperature growth of Ge on Si(100)," Appl. Phys. Lett. **58**(20), 2276–2278 (1991).
7. R. Loiacono, G. T. Reed, G. Z. Mashanovich, R. M. Gwilliam, G. Lulli, R. Feldesh, and R. Jones, "Low-energy silicon-on-insulator ion implanted gratings for optical wafer scale testing," Proc. SPIE **7943**, 794310 (2011).
8. G. Liu and S. J. Fonash, "Selective area crystallization of amorphous silicon films by low-temperature rapid thermal annealing," Appl. Phys. Lett. **55**(7), 660–662 (1989).
9. S. Nishida, T. Shiimoto, A. Yamada, S. Karasawa, M. Konagai, and K. Takahashi, "Epitaxial growth of silicon by photochemical vapor deposition at a very low temperature of 200 °C," Appl. Phys. Lett. **49**(2), 79–81 (1986).
10. D. J. Eaglesham, H. J. Gossmann, and M. Cerullo, "Limiting thickness hepi for epitaxial growth and room-temperature Si growth on Si(100)," Phys. Rev. Lett. **65**(10), 1227–1230 (1990).
11. P. M. Waugh, "First order Bragg grating filters in silicon on insulator waveguides," Proc. SPIE **7056**, 70561T (2008).

#199672 - $15.00 USD Received 16 Oct 2013; revised 3 Dec 2013; accepted 8 Dec 2013; published 10 Jan 2014

12. M. P. Bulk, A. P. Knights, P. E. Jessop, P. Waugh, R. Loiacono, G. Z. Mashanovich, G. T. Reed, and R. M. Gwilliam, "Optical filters utilizing ion implanted Bragg gratings in SOI waveguides," Adv. Opt. Technol. **2008**, 276165 (2008).
13. S. Homampour, M. P. Bulk, P. E. Jessop, and A. P. Knights, "Thermal tuning of planar Bragg gratings in silicon-on-insulator rib waveguides," Phys. Status Solidi C **6**(S1), S240–S243 (2009).
14. T. Tamir and S. Peng, "Analysis and design of grating couplers," Appl. Phys. A Mater. Sci. Process. **14**(3), 235–254 (1977).
15. D. Taillaert, P. Bienstman, and R. Baets, "Compact efficient broadband grating coupler for silicon-on-insulator waveguides," Opt. Lett. **29**(23), 2749–2751 (2004).
16. Lumerical, "FDTD Solutions | Lumerical's Nanophotonic FDTD Simulation Software" (Lumerical, 2013), https://www.lumerical.com/tcad-products/fdtd/.
17. K. F. Heidemann, "Complex-refractive-index profiles of 4 MeV Ge ion-irradiation damage in silicon," Philos. Mag. B **44**(4), 465–485 (1981).
18. R. Parke, R. Waarts, D. F. Welch, A. Hardy, and W. Streifer, "High efficiency, high uniformity, grating coupled surface emitting lasers," Electron. Lett. **26**(2), 125–127 (1990).
19. N. Eriksson, M. Hagberg, and A. Larsson, "Highly efficient grating-coupled surface-emitters with single outcoupling elements," IEEE Photonics Technol. Lett. **7**(12), 1394–1396 (1995).
20. X. Chen, C. Li, C. K. Fung, S. M. Lo, and H. K. Tsang, "Apodized waveguide grating couplers for efficient coupling to optical fibers," IEEE Photonics Technol. Lett. **22**(15), 1156–1158 (2010).
21. E. Baranova, V. Gusev, W. Martynenko, C. Starinin, and I. Haibullin, "On silicon amorphization during different mass ion implantation," Radiat. Eff. **18**(1-2), 21–26 (1973).
22. L. A. Christel, J. F. Gibbons, and T. W. Sigmon, "Displacement criterion for amorphization of silicon during ion implantation," J. Appl. Phys. **52**(12), 7143–7146 (1981).
23. H. Cerva and G. Hobler, "Comparison of transmission electron microscope cross sections of amorphous regions in ion implanted silicon with point-defect density calculations," J. Electrochem. Soc. **139**(12), 3631–3638 (1992).
24. J. R. Dennis and E. B. Hale, "Crystalline to amorphous transformation in ion-implanted silicon: a composite model," J. Appl. Phys. **49**(3), 1119–1127 (1978).
25. G. Hobler and G. Otto, "Status and open problems in modeling of as-implanted damage in silicon," Mater. Sci. Semicond. Process. **6**(1–3), 1–14 (2003).
26. O. Engström, S. Bengtsson, G. I. Andersson, M. O. Andersson, and A. Jauhiainen, "Electrical characterization of bonding interfaces," J. Electrochem. Soc. **139**(12), 3638–3644 (1992).
27. G. Lulli, M. Bianconi, A. Parisini, and E. Napolitani, "Structural characterization and modeling of damage accumulation in In implanted Si," J. Appl. Phys. **95**(1), 150–155 (2004).
28. R. Loiacono, G. T. Reed, G. Z. Mashanovich, R. Gwilliam, S. J. Henley, Y. Hu, R. Feldesh, and R. Jones, "Laser erasable implanted gratings for integrated silicon photonics," Opt. Express **19**(11), 10728–10734 (2011).
29. R. Loiacono, R. Topley, A. Nakyobe, G. Mashanovich, R. Gwilliam, G. Lulli, R. Feldesh, R. Jones, and G. Reed, "Very low energy implanted Bragg gratings in SOI for wafer scale testing applications," in *2011 8th IEEE International Conference on Group IV Photonics (GFP)* (2011), pp. 51–53.
30. R. Loiacono, "Erasable Bragg gratings in silicon on insulator," Ph.D thesis (University of Surrey, 2010).
31. G. Lulli, E. Albertazzi, M. Bianconi, R. Nipoti, M. Cervera, A. Carnera, and C. Cellini, "Stopping and damage parameters for Monte Carlo simulation of MeV implants in crystalline Si," J. Appl. Phys. **82**(12), 5958–5964 (1997).
32. G. F. Cembali, P. G. Merli, and F. Zignani, "Self-annealing of ion-implanted silicon: First experimental results," Appl. Phys. Lett. **38**(10), 808–810 (1981).
33. J.A. Woollam Co, Inc.,"Spectroscopic Ellipsometer Software – CompleteEASE," http://www.jawoollam.com/completeease.html, 2013.
34. A. P. Knights, K. J. Dudeck, W. D. Walters, and P. G. Coleman, "Modification of silicon waveguide structures using ion implantation induced defects," Appl. Surf. Sci. **255**(1), 75–77 (2008).
35. S. K. Selvaraja, D. Vermeulen, M. Schaekers, E. Sleeckx, W. Bogaerts, G. Roelkens, P. Dumon, D. Van Thourhout, and R. Baets, "Highly efficient grating coupler between optical fiber and silicon photonic circuit," in *Lasers and Electro-Optics, CLEO/QELS 2009* (IEEE, 2009), pp. 1–2.

1. Introduction

Silicon is one of many materials that are being used to develop integrated optical circuits. By using silicon to develop these circuits, it is possible to adopt well known manufacturing techniques from silicon based microelectronics and transfer them to the manufacture of photonic circuits [1]. This potentially also enables easier integration of electronics and photonics. Coupling of light into a sub-micron waveguide to be used alongside electronics is a non-trivial task [2]; planar waveguides are around two orders of magnitude smaller than a standard fibre based waveguide leading to a large mode mismatch. The most popular

#199672 - $15.00 USD Received 16 Oct 2013; revised 3 Dec 2013; accepted 8 Dec 2013; published 10 Jan 2014

coupling methods used to transfer the optical mode while minimising loss are prism coupling, end-fire coupling and grating coupling [1].

Grating couplers do not require time consuming preparation such as polishing or anti-reflective coatings and can be measured before dicing the wafer, potentially allowing time and cost savings. Grating couplers are formed by a periodic change in the refractive index of the waveguide, typically by utilising an etch process [2, 3], but in the case of this work, utilising a germanium implant. Light is then coupled in or out through the surface at an angle to reduce surface reflections. The advantage obtained from using an implant opposed to using a standard etching approach is garnered from retaining the surface planarity, Chemical Mechanical Polishing (CMP) can be used to planarize circuit topologies but may introduce microcontamination and chemical defects [4], which are undesirable for photonic circuits, but perhaps a bigger advantage is the removal of an additional process (CMP), which would otherwise add time and cost.

A planar surface can be critical for further processing. A planar surface improves the quality of deposited or epitaxially grown layers, hence improving the performance of devices made in these layers [5]. Growth or deposition of high quality material on top of a grating coupler allows multiple active optical layers to be realized for multi-layer integrated optical circuits, with the potential to harness the benefits of a second material platform such as germanium [6]. Due to the amorphous nature of the refractive index change being introduced, it may make these devices erasable via rapid thermal annealing methods which is very useful for wafer scale testing applications [7]. However, this also means that subsequent deposition and epitaxy processes must be constrained to a very low temperature so as not to remove the lattice damage during the process. Crystallisation temperatures as low as 500°C have been demonstrated for amorphous silicon [8]. Traditionally epitaxy is performed at temperatures which greatly exceed this, however films have been shown to grow successfully at temperatures as low as 200°C [6, 9] and even at room temperature for very thin layers [10].

Grating couplers which retain planarity also reduce optical interaction with contaminants on the die surface when compared with the surface relief variety, without the need for additional cladding. This may be useful in lab on a chip or other sensing applications to reduce the effect of the gas or liquid introduced to the die surface from effecting coupling performance. Surface relief gratings are also susceptible to voids from incomplete “filling” when covered in a surface coating, or to accidental contamination into the castellation cavities if not coated.

Bragg gratings which attempt to maintain a planar surface have been demonstrated by several authors using different methods. Waugh demonstrated processes using both thermal oxidisation and implantation of oxygen ions, achieving extinction ratios of 8.5dB and 6.8dB respectively [11]. Bulk et al showed a 10dB suppression of the central wavelength in planar Bragg gratings fabricated by oxygen ion implantation [12], and 5dB in results of self-ion implantation in the same paper. Homampour et al. demonstrated Bragg gratings which retained the surface planarity using self-ion implantation, and also showed thermal tunability of the central wavelength of the grating of 80pm/K [13]. The best results to date for planar Bragg gratings were shown by Loiacono et al. [7], who demonstrated a 25dB extinction ratio using ion implantation of germanium to achieve periodic amorphous silicon regions to form a Bragg grating. Removing the surface perturbation in diffractive grating couplers is the next step in developing optical circuits in which the wafers surface planarity is maintained.

2. Optical simulations

Simulations were performed with a grating coupler configured in an output coupling regime as shown in Fig. 1. The profile of the amorphous regions has been idealised to a rectangular profile for the purpose of simulations.

#199672 - $15.00 USD Received 16 Oct 2013; revised 3 Dec 2013; accepted 8 Dec 2013; published 10 Jan 2014

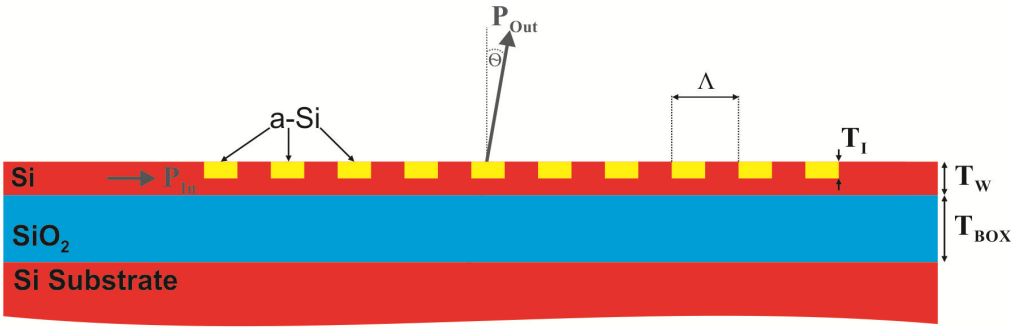

Fig. 1. 2D Simulated implanted grating coupler structure.

A guided mode was launched at P_{In} and subsequently collected at P_{Out}. T_w is the waveguide height and was set at 220nm and T_{BOX} is the buried oxide thickness which was set at 2μm. The grating period is denoted by Λ and implant depth is given by T_I. These parameters were varied to optimise the device. The performance metric used was the output efficiency, η_{out} which is given by Eq. (1).

$$\eta_{out} = \frac{P_{Out}}{P_{In}}. \tag{1}$$

Only the case of the output coupler was considered as grating couplers are reciprocal [14]. Another consideration is that due to the wide waveguide used for a grating coupler (typically 10μm), the effective index does not vary significantly between a 2D and 3D case [15], hence a 2D simulation was used for computational efficiency.

The effective index modulation introduced into the planar style of grating is a periodic increase in the index due to silicon amorphisation as opposed to the surface relief construction which is a periodic reduction in the effective index throughout the grating region. 2D simulations performed in Lumerical's FDTD software package [16] have shown that the extractable optical power from a uniform surface relief grating coupler with a 220nm thick guiding silicon layer is approximately 50% which is in good agreement with [3]. Similar simulations performed for grating couplers formed using lattice disorder show a peak extracted power of 45%. This discrepancy is due to the larger silicon to air Δn of 2.48 afforded by the etch, but suggests both methods of fabrication should offer similar performance characteristics when optimised.

A contour plot was created to aid in device design as shown in Fig. 2. The contour plot shows the output efficiency simulated using Lumerical's FDTD software package [16] for a given grating period and implant depth, based on achieving a Δn of 0.46 in the implanted regions. This refractive index change is shown to be possible in the literature [17]. An implant process to enable operation at any point within this contour map can be designed by selection of the correct implant energy and dose conditions which will be discussed in a later section.

Higher efficiencies have been realized in surface relief gratings using techniques such as substrate reflectors [18, 19], or apodization [20]. These enhancements could be applied to the implanted coupler structure and similar performance improvements would be expected.

Devices in this work have been designed for TE polarization, with grating periods selected around 600nm to achieve a diffraction order of −1.

#199672 - $15.00 USD Received 16 Oct 2013; revised 3 Dec 2013; accepted 8 Dec 2013; published 10 Jan 2014

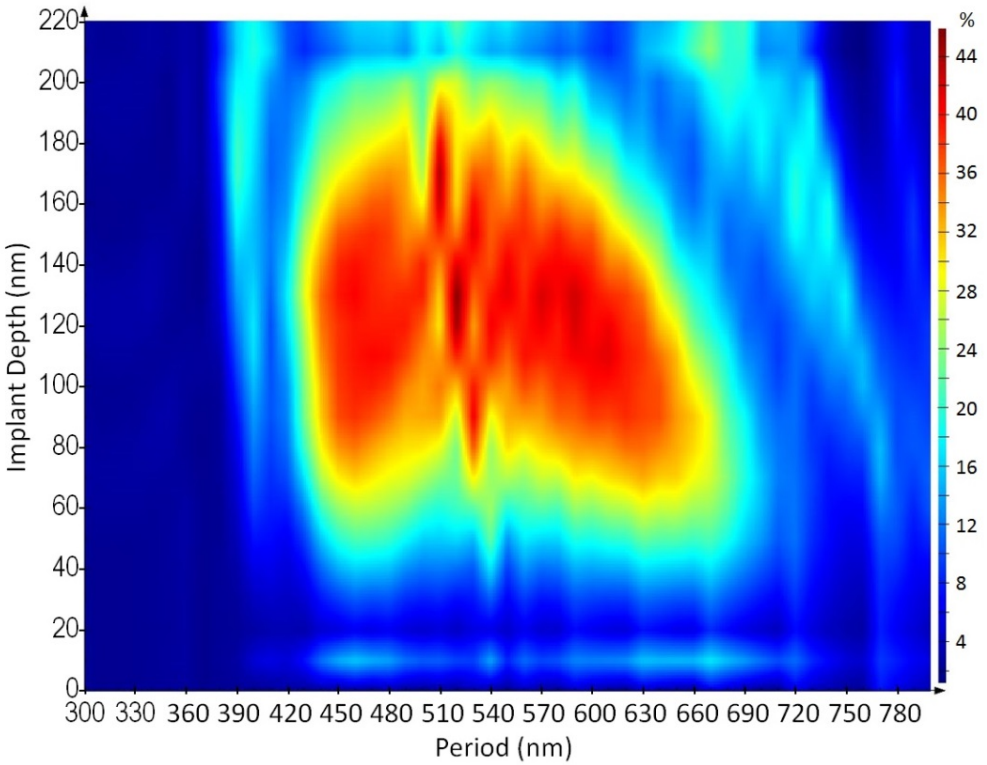

Fig. 2. Contour map of efficiency for various implant depths vs grating period for a 0.5 duty cycle, Ge implanted uniform grating coupler on 220nm SOI with a 2μm buried oxide.

3. Amorphization conditions

The gratings described in this text are formed by periodic regions of amorphous and crystalline allotropes of silicon, patterned to create a modulated effective index due to differing refractive indices of each allotrope. This is because the amorphized regions exhibit a positive Δn compared with crystalline silicon regions. The refractive index change introduced by ion implantation induced lattice disorder in silicon was previously reported in, for example [21]. The threshold level of lattice disorder required for amorphous silicon formation varies in the literature (e.g [22–24].) with a more detailed explanation given in [25]. However, there is a good agreement when the defect density threshold for amorphization is calculated with a defect density model, in that the crystalline – amorphous transition occurs with a critical point defect density of 1.15×10^{22} cm^{-3} [23, 26]. It is also clear from the results of [17], that Δn increases with an increase in dose with a maximum Δn of 0.585 demonstrated.

When considering the ion specie to be used to introduce lattice disorder, it is essential that it is not a silicon dopant, as subsequent thermal treatments may activate the dopant which is likely to have a significant effect on the devices loss characteristics. Restricting the specie selected to a group IV element or a noble gas ensures no doping occurs. Ion species simulated included silicon, carbon, germanium, tin and xenon. Comparing xenon, tin and germanium for instance, to achieve an amorphous depth of 125nm the implant energies required are 142KeV, 133KeV and 90KeV respectively. This shows Xenon and Tin require higher implant energies to achieve the same implant depths as Germanium, higher energies lead to larger degrees of damage broadening under the mask, this results in skewing of the duty cycle and increasing the curvature of the side walls. Germanium was selected as the specie to be implanted as it offers low lateral straggling and also achieves amorphisation with

#199672 - $15.00 USD Received 16 Oct 2013; revised 3 Dec 2013; accepted 8 Dec 2013; published 10 Jan 2014

a relatively low dose condition. Selecting a CMOS compatible element as the ion specie also has benefits in the increased ease of process adoption.

The amount of disorder accumulated in the lattice is strongly dependant on the sample temperature and implanted dose as well as the implanted ion mass. The dose used in this work was 1 x 10^{15} ions cm^{-2} and implants were performed at room temperature.

The ion implantation process was simulated using the King and King 3D software packages, utilising the Monte-Carlo Binary Collision Approximation method [27]. The King software package can quickly and efficiently simulate the depth and level of lattice disorder, whilst King 3D can expand on this information with a more lengthy simulation to show the 3D disorder profile with greater accuracy. Using this software, a simulated level of 80% lattice disorder represents amorphisation with the desired change in refractive index of approximately 0.5, this has been shown to be in good agreement with the damage profiles observed by TEM imagery [28–30].

The simulated optical response shown in Fig. 2 demonstrates that the amorphous depth for optimal performance of a uniform implanted grating coupler with a duty cycle of 0.5, is around 130nm. King simulations show that this corresponds to an implant energy of 100keV which, in simulations achieves an amorphous thickness of 131nm for a dose of 1 x 10^{15} ions cm^{-2}. Having approximately established the parameters to meet the amorphisation depth requirement, a King 3D simulation can be performed as shown in Fig. 3.

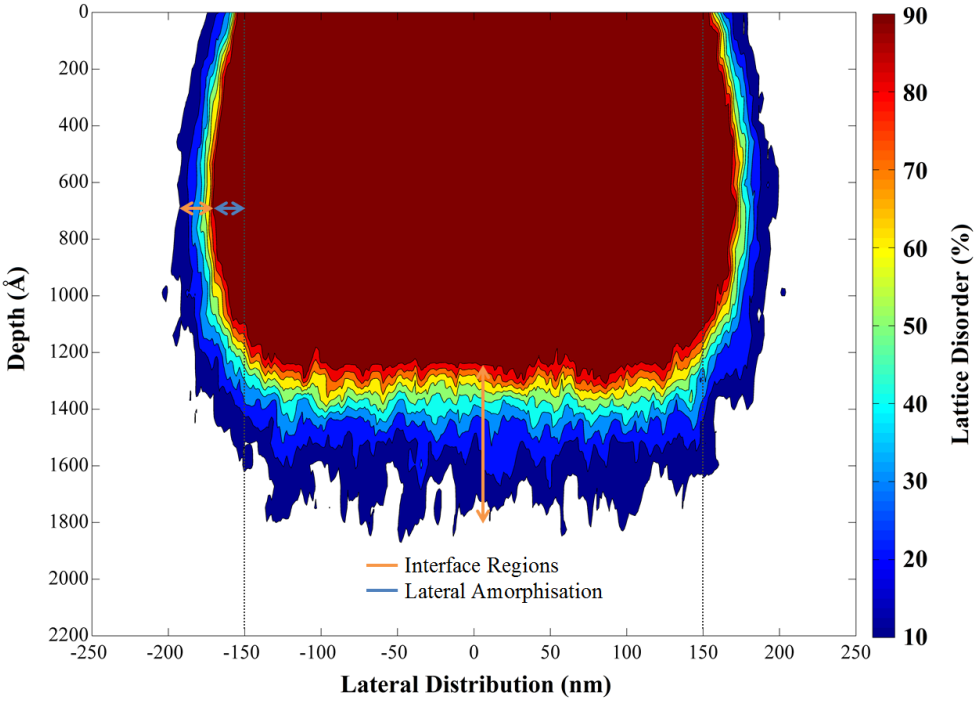

Fig. 3. Amorphization profile for 100 keV energy, 1x10^{15} ions cm^{-2}, implanted through a 300nm slit. Dotted lines represent the width of the mask used.

The full implant profile for a 100keV King 3D simulation with a dose of 1x10^{15} is shown in Fig. 3. King (2D) and King 3D use a Monte-Carlo Binary Collision approximation method for simulation, which does not account for dynamic annealing and the transport of defects [31], hence the simulation must be considered to be most accurate for low temperatures (77K). The simulation highlights large interface regions of lattice disorder, which are neither fully amorphous nor crystalline. Interface regions can be substantially reduced by implanting at room temperature. When the implant is performed at room temperature these regions are not present due to dynamic annealing effects which occur during implantation [32], as

#199672 - $15.00 USD Received 16 Oct 2013; revised 3 Dec 2013; accepted 8 Dec 2013; published 10 Jan 2014

verified via TEM images of similar implant designs [28, 29]. Utilising room temperature implantation also reduces the time and cost of the implantation process. However, 22nm lateral amorphisation above the 80% damage threshold is evident which will alter the effective duty cycle of the implanted devices compared with the mask template, and consequently the optical simulations. A 600nm grating period with a mask duty cycle of 0.5 would give an effective duty cycle of 0.54. This does not reduce efficiency significantly in simulations in this case, though the duty cycle variation may have a greater impact on an apodised grating coupler due to the smaller feature sizes involved. Consequently, the device duty cycle can easily be designed by appropriate modification of the duty cycle in the mask design if required.

4. Processing and fabrication

The processing steps used in fabrication are shown in Fig. 4. Initially the waveguide is fabricated and an e-beam resist is spun onto the wafer. The resist selected was ZEP 520A, spun at 2000rpm to achieve a thickness of 500nm. The waveguide sections are 220nm high silicon wire waveguides with a 400nm width to ensure single mode operation; the buried silicon dioxide layer had a thickness of 2μm. The waveguide grating width is increased to 10μm via a dual step taper to maximise the overlap integral between the fibre and waveguide grating modes, and to facilitate straightforward alignment between fibre and grating. The taper is designed in 2 stages; the flare angle from 10μm to 3μm is set at 0.6° and the angle from 3μm to 400nm at 0.2°.

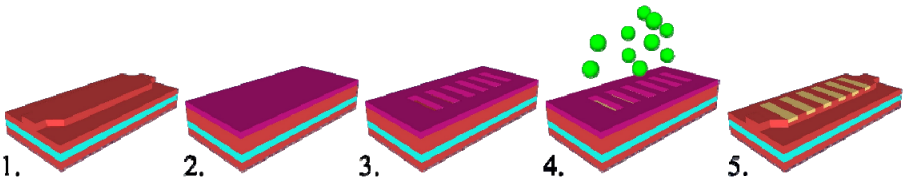

Fig. 4. Device fabrication process: 1. Waveguide etch, 2. Resist spin, 3. Pattern and develop resist, 4. Introduction of lattice disorder, 5. Resist removal.

The e-beam resist is patterned using electron beam lithography and developed to form an ion implantation mask, and subsequently the entire structure is implanted with germanium ions to a dose of 1×10^{15} ions cm^{-2} to ensure amorphisation as discussed in the previous section. The resist was then removed using a 3 stage clean of isopropanol, acetone and deionised water, followed by a 10 minute process in an oxygen plasma asher, the process was carried out at 200°C with an oxygen flow rate of 800ml/min with an RF power of 800W. Following resist removal, the amorphous grating is then ready to use. Using resist as opposed to a hard mask to control the implant reduces the number of process steps required making this process relatively quick and inexpensive.

5. Experimental results

The fabricated amorphous silicon layer thickness and refractive index profile was measured using ellipsometry on a bulk implanted substrate, at 6 different angles of incidence. The data was amalgamated using CompleteEASE® software [33] and fitted using a B-Spline numerical analysis. The amorphized silicon layer thickness was found to be in good agreement with simulated data, with a measured difference between simulation and measurement of below 3nm. The refractive index of the amorphous layer at a wavelength of 1.55μm was found to be 3.96 yielding a Δn of 0.48, which is in good agreement with the expected Δn of up to 0.585 from other literature [17, 28, 34].

Implanted couplers were measured at a 17° angle of incidence to minimise back reflection. Five gratings were fabricated with periods of 580, 590, 600, 610 and 620nm all with the same 0.5 resist mask duty cycle. Surface relief gratings were also designed and

#199672 - $15.00 USD Received 16 Oct 2013; revised 3 Dec 2013; accepted 8 Dec 2013; published 10 Jan 2014

fabricated for comparison, with waveguides and tapers identical to those used for the implanted structures. A period of 700nm and an etch depth of 70nm were used. The most efficient surface relief grating coupler and taper combination exhibited a coupling loss of 4.5dB which is comparable to the best amorphous silicon grating coupler with taper structure of 5.5dB, as shown in Fig. 5.

The 1dB and 3dB bandwidth of the implanted devices are 32nm and 56nm respectively. The corresponding bandwidths of the surface relief gratings fabricated alongside the implanted versions were measured to be 30nm and 51nm respectively, which is comparable to uniform surface relief gratings published in the literature [15, 35].

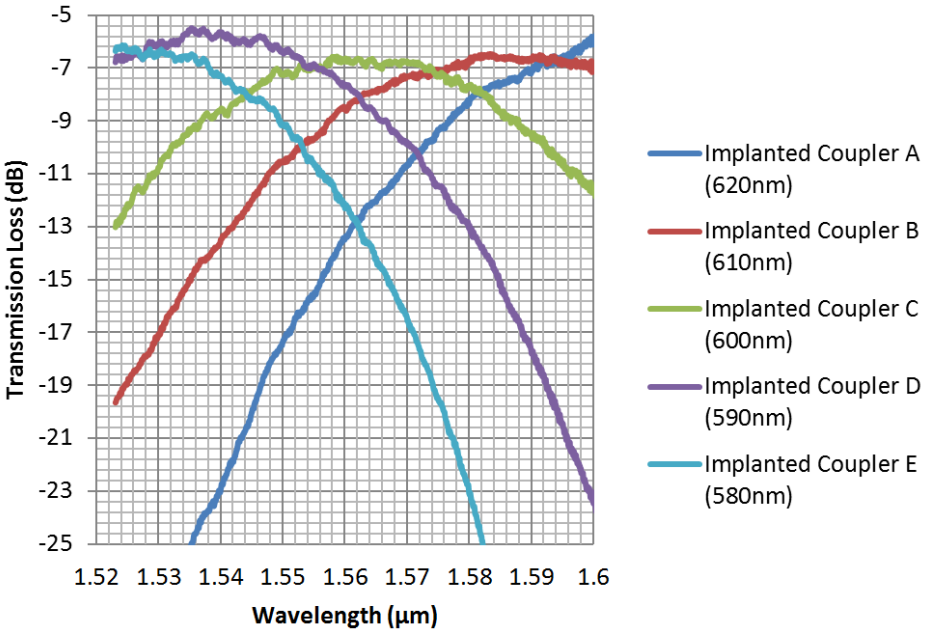

Fig. 5. Performance of implanted grating couplers at different central wavelengths.

The implanted structures perform comparably with surface relief gratings as expected. The Δn of 0.48 introduced by the amorphous to crystalline interface is considerably lower than that of the silicon to air, or silicon to silicon dioxide, with Δn of 2.48 and 1.95 respectively. A lower index contrast reduces coupling strength, to compensate for this, the amorphous region is almost twice as deep as the comparable etched region, maximising the effective index contrast. This results in the performance of the implanted coupler being only 1dB lower than the surface relief counterpart.

6. Conclusions

In this paper a novel method of fabrication has been demonstrated for diffractive grating couplers which allow the surface planarity of silicon waveguide devices to be maintained whilst still providing comparable coupling efficiency between a silicon wire waveguide and a single mode optical fibre, as compared to a surface relief grating. The effective index modulation introduced via ion implantation forms an amorphous allotrope of silicon using lattice disorder.

The coupling loss for an implanted grating and taper combination shows a performance reduction of only 1dB compared with its etched counterpart and the 1dB and 3 dB bandwidths are also shown to be comparable to those of surface relief gratings.

Acknowledgments

The authors would like to thank EPSRC, UK for funding this work. Goran Mashanovich would like to acknowledge support from the Royal Society.

#199672 - $15.00 USD Received 16 Oct 2013; revised 3 Dec 2013; accepted 8 Dec 2013; published 10 Jan 2014